Incoherent Cooper pairing and pseudogap behavior in single-layer FeSe/$SrTiO_3$- SUPPLEMENTAL INFORMATION

B.D. Faeth,[1] S.-L. Yang,[1,2,3] J.K. Kawasaki,[1] J.N. Nelson,[1] P. Mishra,[1] C.T. Parzyck,[1] C. Li,[1] D.G. Schlom,[3] and K.M. Shen[1,2]

[1]*Department of Physics, Laboratory of Atomic and Solid State Physics, Cornell University, Ithaca, New York 14853, USA*
[2]*Kavli Institute at Cornell for Nanoscale Science, Ithaca, NY 14853, USA*
[3]*Department of Materials Science and Engineering, Cornell University, Ithaca, NY 14853, USA*

(Dated: April 16, 2021)

I. EVALUATION OF *IN SITU* CONTACT RESISTANCE AND DETERMINATION OF R_s

To ensure that our *in situ* resistivity measurements are not influenced by loss of electrical contact with the monolayer films, we simultaneously measure 2-point electrical resistances across all available lead pairs during 4-point $R(T)$ measurement using a Keithley 3706 matrix relay board. Figure S1 shows comprehensive 2 and 4-point $R(T)$ and $V(I)$ characteristics for a representative single-layer FeSe/$SrTiO_3$ film as measured through the superconducting transition. Within this range of applied current values ($|I| \leq 50$ μA, well below I_c) the $V(I)$ curves remain linear for all measured pairs both below and above the onset of zero resistance at T_0, indicating reliable ohmic contact. For $T < T_0$, 2-point resistances are measured to be ≈ 100 Ω [Fig. S1(b)], implying typical contact resistances in the range of ≈ 50 Ω per probe. Additionally, the resistance to ground across all contacts are checked and confirmed to remain open throughout measurements. Together, this characterization ensures that our *in situ* transport measurements reflect the intrinsic behavior of only the isolated single layer FeSe.

Some anisotropy is present in the shape of the resistive transitions for the perpendicular 4-point configurations $I_{13}V_{24}$ versus $I_{12}V_{34}$, as shown in Figure S1(a). As monolayer FeSe/$SrTiO_3$ remains epitaxially locked into the tetragonal phase down to low temperature, we speculate that anisotropy may be instead due to the relative orientation of the current direction compared to the $SrTiO_3$ step edges, which can act as scattering planes. Similar behavior has been previously reported for for $(\sqrt{7} \times \sqrt{3})$-In surface reconstructions on Si(111) [1] as well as in ultra-thin metallic Ga [2]. To minimize the influence of such an effect on our results, sheet resistance values reported here are calculated using the preferred (lower resistance) direction such that:

$$R_s = \frac{1.34\pi}{\ln(2)} \frac{V_{24}}{I_{13}}, \tag{1}$$

where $\frac{\pi}{\ln(2)}$ is the Van der Pauw factor and 1.34 is an additional factor to account for the finite contact dimensions based on the known dimensions of the Au electrodes [3]. For films measured without gold electrodes present, we instead use a correction factor of 1.1, based on a finite-element analysis of the Van der Pauw correction factor for our known probe geometry.

For $V(I)$ measurement, to minimize potential sample heating effects, a pulse-current measurement mode with a low duty cycle (0.2%) is utilized. In this mode the measurement current is applied in short duration pulses separated in time by some pulse interval, as shown in Fig. S2(a). Prior to final measurement, current pulse settings are calibrated by sweeping the pulse interval and width [Fig. S2(b,c)], and selecting pulse parameters such that the nonlinear deviation at high current is minimized. For the data shown in Figure 3, we use a pulse width of 1 ms with an interval of 500 ms, where the pulse amplitude is stepped from 1 uA to an instrumentally limited value of 10 mA.

II. FITTING OF THE SUPERCONDUCTING TRANSITION TO THE BEREZINSKII-KOSTERLITZ-THOULESS AND AZLAMAZOV-LARKIN MODELS

Two-dimensional superconductors exhibit a complicated critical phenomenology compared to the conventional 3D case; in the following section we consider the underlying mechanism of 2D phase fluctuations and its implications on the transport and ARPES behavior we observe in single-layer FeSe/$SrTiO_3$ films.

In the 2D limit the long-range correlation of the superconducting order parameter is famously prohibited by the Mermin-Wagner theorem [4]; instead 2D superconductors exhibit a Berezinskii-Kosterlitz-Thouless (BKT) type phase transition [5], which allows for the establishment of a quasi-long-range order only at some T_{BKT} below the mean-field pairing temperature T_c. The 2D BKT superconducting state is characterized by the binding of vortex-antivortex pairs (vortices with opposite supercurrent circulation). Whereas unpinned free vortexes produce energy dissipation (and thus a finite resistance) as a result of flux flow (as in a conventional type-II superconductor), bound vortex pairs experience no net Lorentz force from a transport current, and thus allow for dissipation-free transport. Below the critical temperature T_{BKT}, the thermal energy is insufficient to break bound antiparallel vortex pairs, and thus the system will exhibit zero electrical resistance in the absence of external perturbation. A finite applied current will disassociate vortex pairs, generating free vortices and subsequently a voltage response in the form of:

$$V \propto I^{\alpha(T)}, \quad T < T_{BKT}, \tag{2}$$

where $\alpha(T)$ is proportional to the number of unbound vortices times the drift rate across the current. Just at the transition point this is predicted to result in $\alpha(T_{BKT}) = 3$ [6].

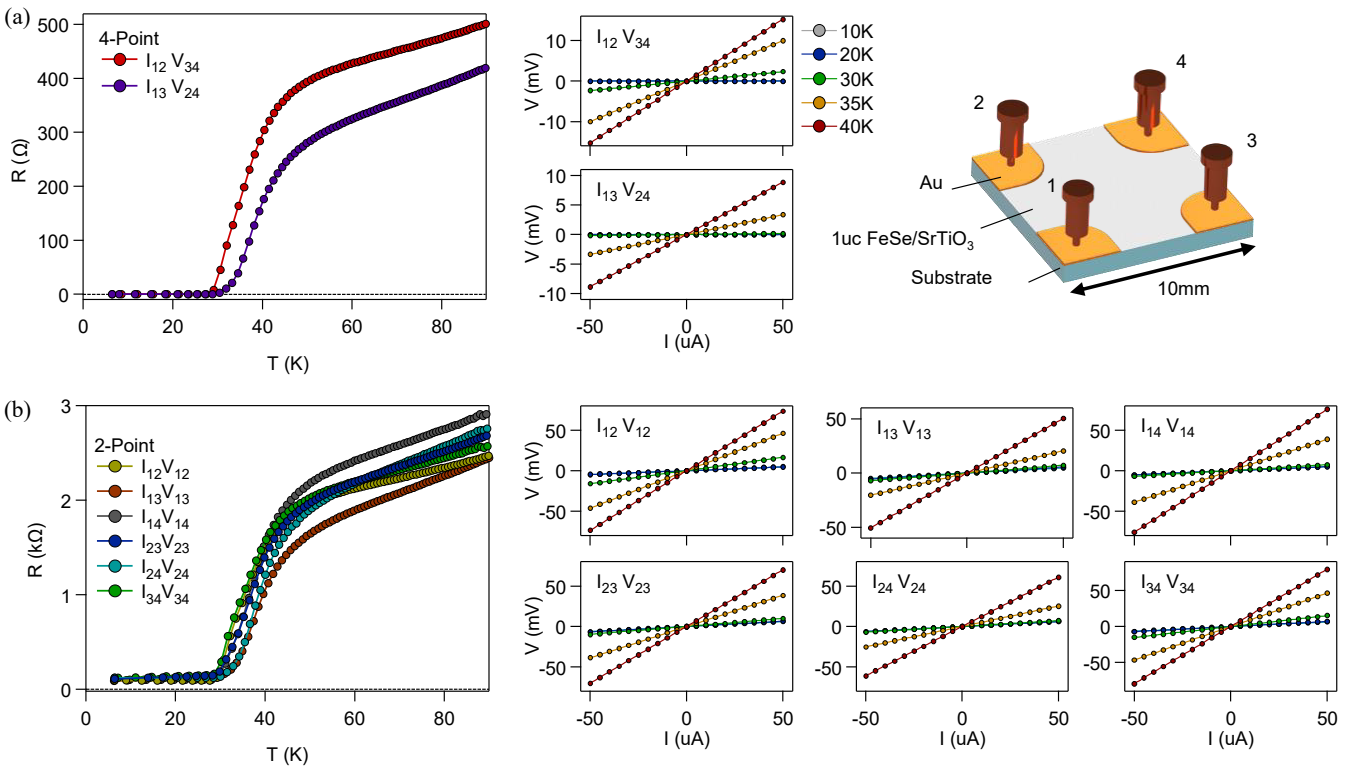

Figure S1. **Evaluation of the contact resistances during in situ $R(T)$ measurements on a representative 1uc FeSe/SrTiO$_3$ film.** (**a**) 4-point measurements taken along orthogonal directions in the Van der Pauw geometry. The left panel displays the resistance measured using the Delta mode while the right panels show the voltage response in current-pulse mode at various temperatures across the transition. The diagram in the upper right panel shows the index convention used for the contact probes. (**b**) Equivalent 2-point resistances (left panel) and V(I) behavior (right panels) measured between each pair of contacts, including lead and contact resistances.

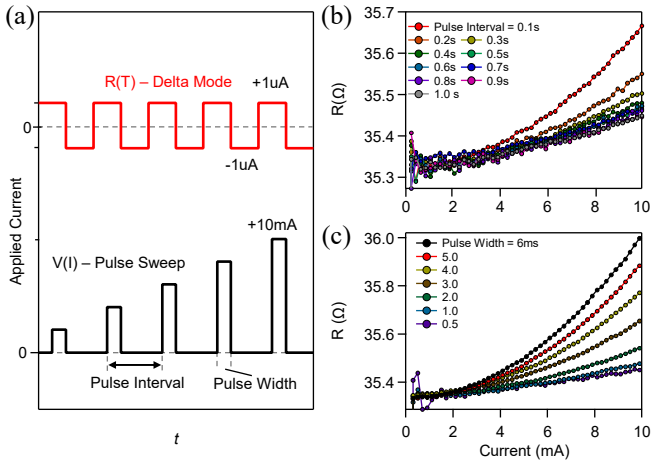

Figure S2. **Heating effects during V(I) measurements.** (**a**) Diagram showing measurement modes used for R(T) (red) and V(I) (black) measurements shown throughout the text. (**b,c**) Measured resistance of a representative 1uc FeSe/SrTiO$_3$ film held above T_0 as a function of applied current in Pulse Sweep mode. For shorter pulse intervals (**b**) or longer pulse widths (**c**) some heating effects are evident.

Above T_{BKT} the proliferation of thermally excited free vortices leads to a linear resistance from vortex flux flow, such that $\alpha(\mathrm{T}>T_{BKT}) = 1$.

At low applied currents the emergent flux-flow resistance is related to the density of thermally-populated free vortices n_F, which we can define in terms of a correlation length $\xi^2 = 1/(2\pi n_F)$, analogous to the Ginzburg-Landau coherence length ξ_0 for Cooper pairs; at separations less than ξ, vortices remain bounded in pairs, even above T_{BKT}. At T_{BKT}, ξ diverges, thus all vortices are paired. For comparison to *in situ* transport measurements, we can express this in terms of the excess conductivity $\Delta\sigma$ in the BKT vortex state compared to the normal state σ_n. Above T_{BKT} it can be shown [7] that the excess conductivity exhibits exponential behavior related to the density of thermally generated vortices:

$$\frac{\Delta\sigma_{BKT}}{\sigma_n} = \left(\frac{\xi}{\xi_0}\right)^2 = Ae^{b/\sqrt{t}}, \quad T_{BKT} < T < T_c. \quad (3)$$

Thus the intermediate vortex state may produce a substantially broadened superconducting transition.

Additionally, two-dimensional superconductors may intrinsically exhibit greatly enhanced amplitude fluctuations [8] which manifest as short-lived, uncondensed Cooper pairs above T$_c$ that contribute to both the density of states and con-

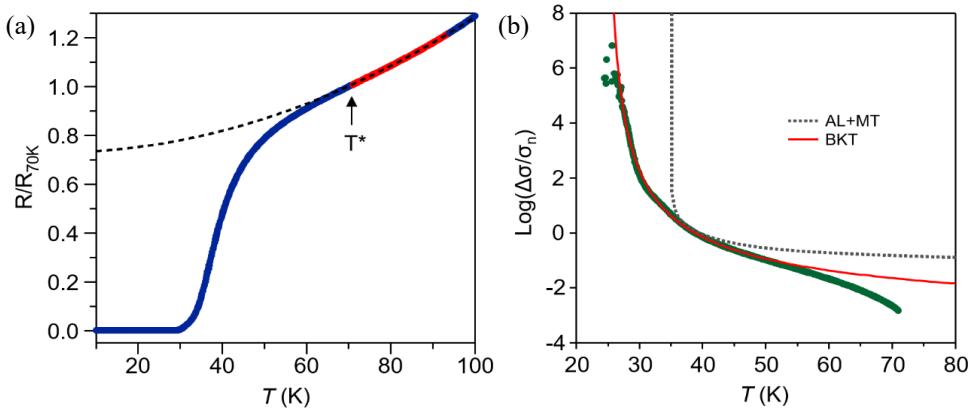

Figure S3. **Fitting of the superconducting transition to BKT and AL paraconductivity models.** (**a**) *in situ* resistivity data from Figs. 1 and 2 of the main text, normalized to the resistance at 70 K. (b) The excess conductivity extracted from the data in panel (a). Dashed black and red lines show fits to the AL+MT paraconductivity and BKT models, respectively.

duction. The contribution of thermally populated cooper pairs to the conduction is described by the Aslamazov–Larkin (AL) paraconductivity:

$$\Delta\sigma_{\mathrm{AL}} = \frac{e^2}{16\hbar}\frac{T_c}{T-T_c}, \quad T > T_c, \tag{4}$$

with an additional term for the Maki-Thomson correction [9, 10] included as

$$\Delta\sigma_{\mathrm{MT}} = \frac{e^2}{8\hbar}\frac{T_c}{T-(1+\delta)T_c}\ln\frac{T-T_c}{\delta T_c}, \quad T > T_c. \tag{5}$$

In Figure S3 we compare fits of the superconducting transition in single-layer FeSe/$SrTiO_3$ measured by *in situ* transport to the BKT and AL+MT models described by equations 4 and 5. Figure S3(a) shows R_s(T) for the single-layer film as presented in Figs 1-3 of the main text. The normal-state resistance (black dashed line) is extrapolated from Rs above T* (red region). Fig. S3(b) shows the normalized excess conductivity in log scale (green), along with fits to the BKT model (red line) and the AL paraconductivity (black dashed line). As shown, the AL+MT fitting fails to reproduce the shape of R_s(T) seen in our films, both at low temperatures approaching T_0 and the steeper downwards slope at higher temperatures.

III. MEASUREMENT AND EVALUATION OF THE SUPERCONDUCTING ENERGY GAP

Figure S4 outlines the procedure used to generate detailed temperature-dependent gap measurements as shown in Figure 2. The film is gradually warmed from 12-94 K while continuously measuring ARPES spectra at M [Fig. S4(d,e)]. The Fermi level is determined by periodically measuring reference spectra on the amorphous Au electrodes (in direct electrical and thermal contact with the FeSe film). Fig. S4(c) shows angle-integrated (normalized) spectra for Au at different temperatures through the sweep. The energy resolution and temperature are estimated based on a fitting of the integrated Au spectra to the Fermi function. Measured EDCs at k_F [Fig. S4(f) are symmetrized about E_F to generate the data in Fig. 2(a,b).

One approach to evaluating the superconducting energy gap Δ is to fit the symmetrized EDC's at E_F to a model spectral function with a self-energy in the form of

$$\Sigma(\mathbf{k}, E) = -i\Gamma_1 + \frac{\Delta^2}{[E+\epsilon(\mathbf{k})+i\Gamma_0]}, \tag{6}$$

where Γ_0 is the inverse pair lifetime, Γ_1 describes the single-particle scattering rate, and $\epsilon(\mathbf{k})$ is the bare band dispersion. The corresponding spectral function is then calculated as

$$A(\mathbf{k}, E) = -\frac{1}{\pi}\frac{\Sigma''(\mathbf{k}, E)}{\left[E-\epsilon(\mathbf{k})-\Sigma'(\mathbf{k}, E)\right]^2+\Sigma''(\mathbf{k}, E)^2}, \tag{7}$$

and convolved with a gaussian with full width at half maximum (FWHM) matching the experimental energy resolution to produce a model spectral function for gap fitting. This method accounts for artificial broadening of the photoemission spectra due to energy resolution and scattering effects, and has been used previously in studies of high-T_c superconductors and monolayer FeSe/$SrTiO_3$ [11, 12].

At low temperatures, where the sample is deep within the superconducting state, Γ_0 can be reasonably assumed to be 0, and a fit of the form of Eqs. S5 and S6 can be performed reliably. Near the gap closing temperature and in the presence of superconducting fluctuations, however, the assumption that $\Gamma_0 = 0$ no longer holds, and a fitting of the form of Eqs. S5 and S6 becomes poorly constrained: both $\Delta = 0$ or an excessive Γ_0 produce fully "filled" spectral functions. As we are more

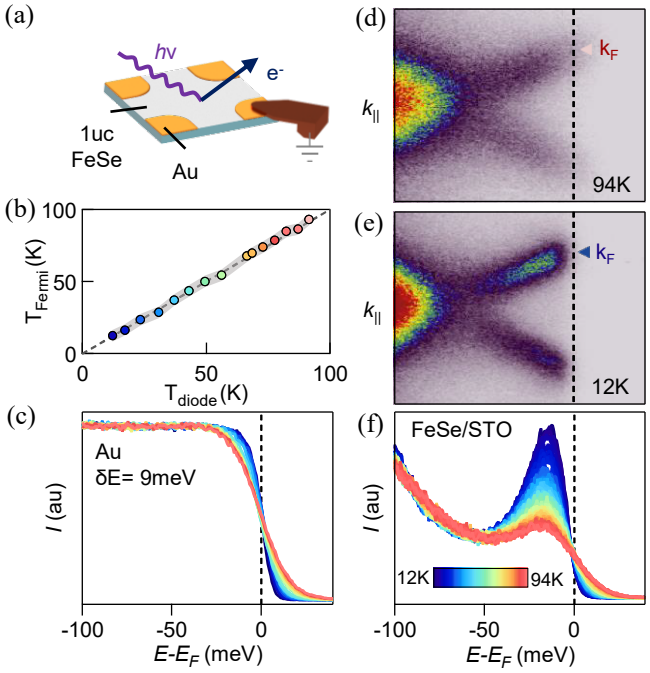

Figure S4. **ARPES gap measurements and temperature evaluation.** (**a**) Measurement configuration for ARPES gap measurements. The sample is grounded using a press contact built onto the sample manipulator. (**b**) The sample temperature evaluated from a fit to the Fermi edge of the Au electrodes, as shown in (**c**), compared to the sample diode reading. (**d-f**) Temperature evolution of the ARPES spectra at M. The data in Panel F is equivalent to that shown in Figure 2(b) without symmetrization.

concerned with the presence of an energy gap (as a signature of incoherent cooper pairs), we use instead the peak separation to characterize Δ(T) for the entire temperature range in the main text, particularly in Fig. 2(c). The gap-opening temperature T_Δ is identified as the maximum temperature at which separated quasiparticle peaks are distinguishable above the measurement noise [Fig. S5(c)].

To ensure that our estimation of T_Δ is not skewed by our methodology, we have tested using the spectral-function fitting approach as well, allowing Γ_0, Γ_1, and Δ to remain unconstrained fitting parameters, as shown in Figure S5.

IV. DATA FROM ADDITIONAL SAMPLES

The data shown in Fig. 4(b) and Fig. 4(c) of the main text is compiled from many single-layer FeSe/$SrTiO_3$ samples for which temperature-dependent transport data is available. Of these, low-temperature ARPES data were also available on five films, and temperature-dependent data for four. Figure S6 presents temperature-dependent symmetrized EDC's at k_F for the additional films not presented in the main text, but included in Fig. 4. T_Δ for each sample was determined via the same approach as used in Fig. 2 of the main text. Despite variation in the disorder strength, all films show qualitatively similar behavior to that of the film presented in Fig. 2, namely the distinct filling of spectral weight at E_F at low temperatures, as well as comparable T_Δ values.

Fig. S7 shows dR_s/dT data for the same selection of metallic (positive dR_s/dT at all temperatures) films presented in Fig.4(a). Fig. S7(a) shows full data out to 150 K, and Fig. S7(b) shows a zoom-in on the region near T^*.

[1] Takashi Uchihashi, Puneet Mishra, Masakazu Aono, and Tomonobu Nakayama, "Macroscopic Superconducting Current through a Silicon Surface Reconstruction with Indium Adatoms: $Si(111)-(\sqrt{7}\times\sqrt{3})-In$," Phys. Rev. Lett. **107**, 207001 (2011).

[2] Natalie Briggs, Brian Bersch, Yuanxi Wang, Jue Jiang, Roland J. Koch, Nadire Nayir, Ke Wang, Marek Kolmer, Wonhee Ko, Ana De La Fuente Duran, Shruti Subramanian, Chengye Dong, Jeffrey Shallenberger, Mingming Fu, Qiang Zou, Ya-Wen Chuang, Zheng Gai, An-Ping Li, Aaron Bostwick, Chris Jozwiak, Cui-Zu Chang, Eli Rotenberg, Jun Zhu, Adri C. T. van Duin, Vincent Crespi, and Joshua A. Robinson, "Atomically Thin Half-Van der Waals Metals Enabled by Confinement Heteroepitaxy," Nature Materials **19**, 637–643 (2020).

[3] Ronald Chwang, B.J. Smith, and C.R. Crowell, "Contact Size Effects on the van der Pauw Method for Resistivity and Hall Coefficient Measurement," Solid-State Electronics **17**, 1217 – 1227 (1974).

[4] N. D. Mermin and H. Wagner, "Absence of Ferromagnetism or Antiferromagnetism in One- or Two-Dimensional Isotropic Heisenberg Models," Phys. Rev. Lett. **17**, 1133–1136 (1966).

[5] J. M. Kosterlitz and D. J. Thouless, "Ordering, Metastability and Phase Transitions in Two-Dimensional Systems," Journal of Physics C Solid State Physics **6**, 1181–1203 (1973).

[6] J M Kosterlitz, "The Critical Properties of the Two-Dimensional xy Model," Journal of Physics C: Solid State Physics **7**, 1046–1060 (1974).

[7] L. Benfatto, C. Castellani, and T. Giamarchi, "Broadening of the Berezinskii-Kosterlitz-Thouless Superconducting Transition by Inhomogeneity and Finite-Size Effects," Phys. Rev. B **80**, 214506 (2009).

[8] Anatoly Larkin, Andrei Varlamov, and James Annett, "Theory of Fluctuations in Superconductors," Physics Today **59** (2006).

[9] Kazumi Maki, "The Critical Fluctuation of the Order Parameter in Type-II Superconductors," Progress of Theoretical Physics **39**, 897–906 (1968).

[10] J. W. P. Hsu and A. Kapitulnik, "Superconducting Transition, Fluctuation, and Vortex Motion in a Two-Dimensional Single-Crystal Nb Film," Phys. Rev. B **45**, 4819–4835 (1992).

[11] Q. Song, T. L. Yu, X. Lou, B. P. Xie, H. C. Xu, C. H. P. Wen, Q. Yao, S. Y. Zhang, X. T. Zhu, J. D. Guo, R. Peng, and D. L. Feng, "Evidence of Cooperative Effect on the Enhanced Superconducting Transition Temperature at the FeSe/$SrTiO_3$ Interface," Nature Communications **10**, 758 (2019).

[12] M. R. Norman, M. Randeria, H. Ding, and J. C. Campuzano, "Phenomenology of the Low-Energy Spectral Function in High-T_c Superconductors," Phys. Rev. B **57**, R11093 (1998).

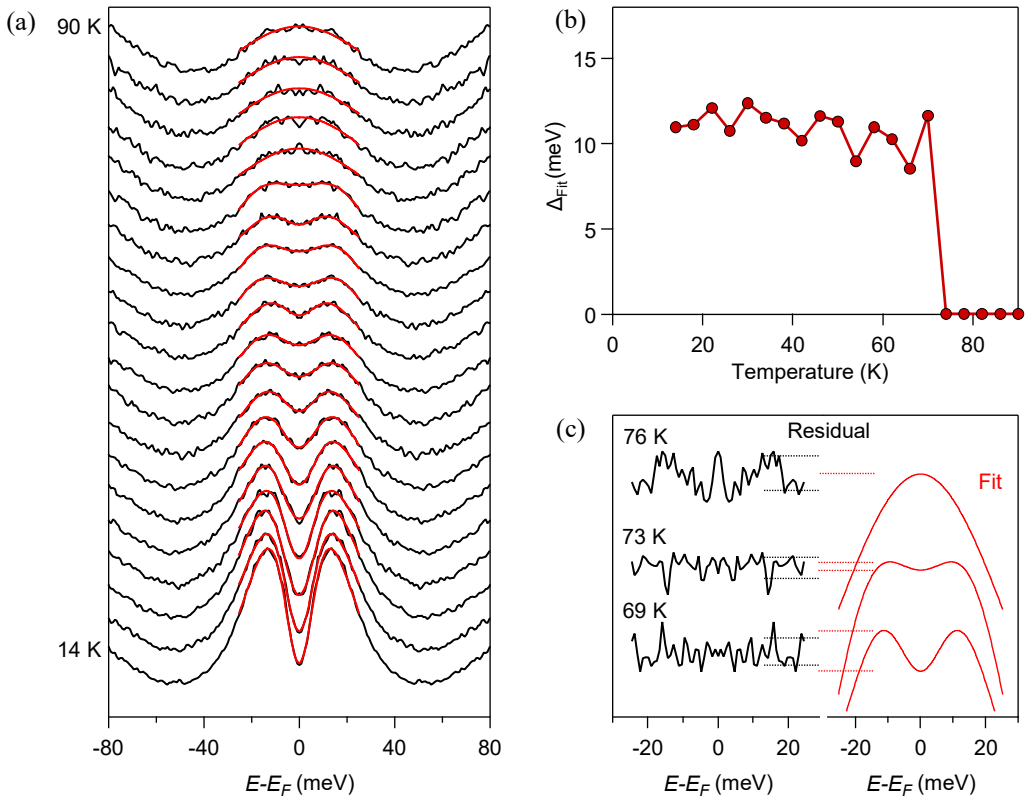

Figure S5. **Fitting of the superconducting gap** (**a**) Temperature-dependent EDC's duplicated from Fig. 2(b), along with fits to the spectral function of Eqs. 6 and 7. (**b**) Δ(T) from fits in panel (a) (**c**) Comparison of EDC gap fits (red) to the residual noise (black) for temperatures near T_{Δ}.

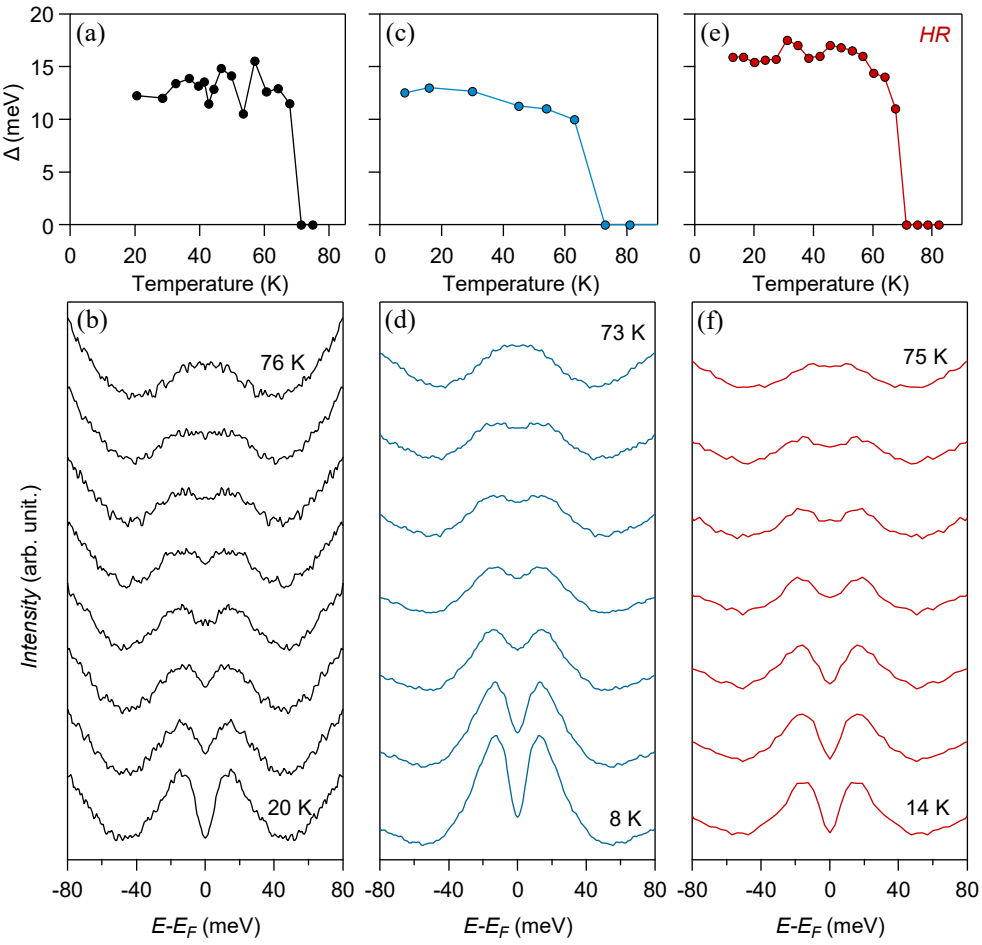

Figure S6. **Temperature-dependent EDC's for additional single-layer FeSe/$SrTiO_3$ films.** Data shown for 3 separate films not previously presented in the main text, including temperature-dependent EDC's at k_F (b,d,f) and corresponding Δ(T) based on quasiparticle peak separation (a,c,e). For films (a) and (e), only a sampling of the total measured EDC's are presented.

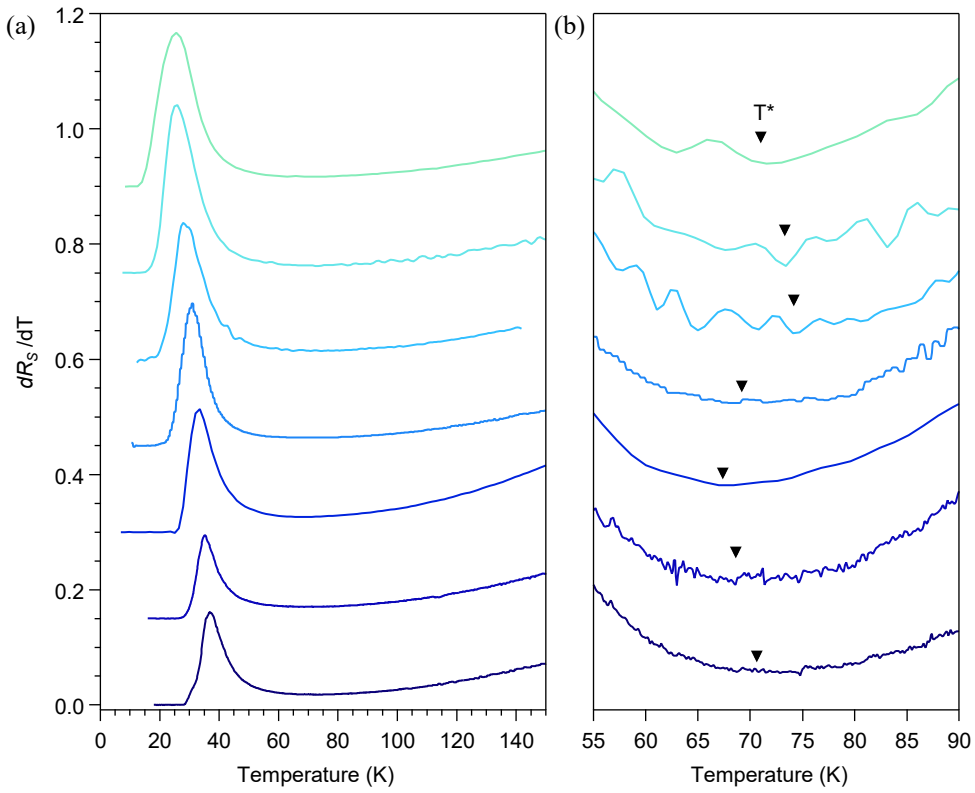

Figure S7. **dR$_s$/dT for additional superconducting single-layer FeSe/SrTiO$_3$ films.** (**a**) dR$_s$/dT for the metallic, superconducting films for which R$_s$(T) was presented in Fig. 4(a) of the main text. (**b**) Zoom-in near T_Δ for the data shown in (a). Arrows indicate the extracted values of T_Δ for each curve.